EUROPEAN ORGANIZATION FOR NUCLEAR RESEARCH

CERN–EP/99-134

26 January 2000
Revised

Measurement of the strange quark forward-backward asymmetry around the Z^0 peak

DELPHI Collaboration

Abstract

A precise measurement of the strange quark forward-backward asymmetry used 3.2M multihadronic events around the Z^0 peak collected by the DELPHI experiment from 1992 to 1995. The ring imaging Cherenkov detectors in the barrel and end-cap regions identify high energy charged kaons which tag the s quark. The s quark asymmetry was measured at different centre-of-mass energies; in particular at the Z^0 pole

$$A^0_{s\bar{s}} = 0.1008 \pm 0.0113\,(\text{stat.}) \pm 0.0040\,(\text{syst.}), \quad (1)$$

taking the expected d and u quark asymmetries from the Standard Model. The quark flavour fractions are assumed from the Standard Model and the fragmentation process is modelled by JETSET. From the s quark pole asymmetry the electroweak mixing angle was determined:

$$\sin^2\theta^{lept}_{eff} = 0.2321 \pm 0.0029. \quad (2)$$

The parity violating coupling of the s quark to the Z was determined to be:

$$A_s = 0.909 \pm 0.102\,(\text{stat.}) \pm 0.036(\text{syst.}). \quad (3)$$

(Accepted by E. Phys. J. C)

P.Abreu[22], W.Adam[52], T.Adye[38], P.Adzic[12], Z.Albrecht[18], T.Alderweireld[2], G.D.Alekseev[17], R.Alemany[51], T.Allmendinger[18], P.P.Allport[23], S.Almehed[25], U.Amaldi[9], N.Amapane[47], S.Amato[49], E.G.Anassontzis[3], P.Andersson[46], A.Andreazza[9], S.Andringa[22], P.Antilogus[26], W-D.Apel[18], Y.Arnoud[9], B.Åsman[46], J-E.Augustin[26], A.Augustinus[9], P.Baillon[9], P.Bambade[20], F.Barao[22], G.Barbiellini[48], R.Barbier[26], D.Y.Bardin[17], G.Barker[18], A.Baroncelli[40], M.Battaglia[16], M.Baubillier[24], K-H.Becks[54], M.Begalli[6], A.Behrmann[54], P.Beilliere[8], Yu.Belokopytov[9], K.Belous[44], N.C.Benekos[33], A.C.Benvenuti[5], C.Berat[15], M.Berggren[26], D.Bertini[26], D.Bertrand[2], M.Besancon[41], M.Bigi[47], M.S.Bilenky[17], M-A.Bizouard[20], D.Bloch[10], H.M.Blom[32], M.Bonesini[29], W.Bonivento[28], M.Boonekamp[41], P.S.L.Booth[23], A.W.Borgland[4], G.Borisov[20], C.Bosio[43], O.Botner[50], E.Boudinov[32], B.Bouquet[20], C.Bourdarios[20], T.J.V.Bowcock[23], I.Boyko[17], I.Bozovic[12], M.Bozzo[14], M.Bracko[45], P.Branchini[40], R.A.Brenner[50], P.Bruckman[9], J-M.Brunet[8], L.Bugge[34], T.Buran[34], B.Buschbeck[52], P.Buschmann[54], S.Cabrera[51], M.Caccia[28], M.Calvi[29], T.Camporesi[9], V.Canale[39], F.Carena[9], L.Carroll[23], C.Caso[14], M.V.Castillo Gimenez[51], A.Cattai[9], F.R.Cavallo[5], V.Chabaud[9], M.Chapkin[44], Ph.Charpentier[9], L.Chaussard[26], P.Checchia[37], G.A.Chelkov[17], R.Chierici[47], P.Chliapnikov[44], P.Chochula[7], V.Chorowicz[26], J.Chudoba[31], K.Cieslik[19], P.Collins[9], R.Contri[14], E.Cortina[51], G.Cosme[20], F.Cossutti[9], H.B.Crawley[1], D.Crennell[38], S.Crepe[15], G.Crosetti[14], J.Cuevas Maestro[35], S.Czellar[16], M.Davenport[9], W.Da Silva[24], A.Deghorain[2], G.Della Ricca[48], P.Delpierre[27], N.Demaria[9], A.De Angelis[9], W.De Boer[18], C.De Clercq[2], B.De Lotto[48], A.De Min[37], L.De Paula[49], H.Dijkstra[9], L.Di Ciaccio[39,9], J.Dolbeau[8], K.Doroba[53], M.Dracos[10], J.Drees[54], M.Dris[33], A.Duperrin[26], J-D.Durand[9], G.Eigen[4], T.Ekelof[50], G.Ekspong[46], M.Ellert[50], M.Elsing[9], J-P.Engel[10], M.Espirito Santo[22], G.Fanourakis[12], D.Fassouliotis[12], J.Fayot[24], M.Feindt[18], P.Ferrari[28], A.Ferrer[51], E.Ferrer-Ribas[20], F.Ferro[14], S.Fichet[24], A.Firestone[1], U.Flagmeyer[54], H.Foeth[9], E.Fokitis[33], F.Fontanelli[14], B.Franek[38], A.G.Frodesen[4], R.Fruhwirth[52], F.Fulda-Quenzer[20], J.Fuster[51], A.Galloni[23], D.Gamba[47], S.Gamblin[20], M.Gandelman[49], C.Garcia[51], C.Gaspar[9], M.Gaspar[49], U.Gasparini[37], Ph.Gavillet[9], E.N.Gazis[33], D.Gele[10], N.Ghodbane[26], I.Gil[51], F.Glege[54], R.Gokieli[9,53], B.Golob[45], G.Gomez-Ceballos[42], P.Goncalves[22], I.Gonzalez Caballero[42], G.Gopal[38], L.Gorn[1], Yu.Gouz[44], V.Gracco[14], J.Grahl[1], E.Graziani[40], P.Gris[41], G.Grosdidier[20], K.Grzelak[53], M.Gunther Axelsson[50], J.Guy[38], F.Hahn[9], S.Hahn[54], S.Haider[9], A.Hallgren[50], K.Hamacher[54], J.Hansen[34], F.J.Harris[36], V.Hedberg[25], S.Heising[18], J.J.Hernandez[51], P.Herquet[2], H.Herr[9], T.L.Hessing[36], J.-M.Heuser[54], E.Higon[51], S-O.Holmgren[46], P.J.Holt[36], S.Hoorelbeke[2], M.Houlden[23], J.Hrubec[52], M.Huber[18], K.Huet[2], G.J.Hughes[23], K.Hultqvist[46], J.N.Jackson[23], R.Jacobsson[9], P.Jalocha[19], R.Janik[7], Ch.Jarlskog[25], G.Jarlskog[25], P.Jarry[41], B.Jean-Marie[20], D.Jeans[36], E.K.Johansson[46], P.Jonsson[26], C.Joram[9], P.Juillot[10], L.Jungermann[18], F.Kapusta[24], K.Karafasoulis[12], S.Katsanevas[26], E.C.Katsoufis[33], R.Keranen[18], G.Kernel[45], B.P.Kersevan[45], B.A.Khomenko[17], N.N.Khovanski[17], A.Kiiskinen[16], B.King[23], A.Kinvig[23], N.J.Kjaer[32], O.Klapp[54], H.Klein[9], P.Kluit[32], P.Kokkinias[12], M.Koratzinos[9], V.Kostioukhine[44], C.Kourkoumelis[3], O.Kouznetsov[41], M.Krammer[52], E.Kriznic[45], Z.Krumstein[17], P.Kubinec[7], J.Kurowska[53], K.Kurvinen[16], J.W.Lamsa[1], D.W.Lane[1], V.Lapin[44], J-P.Laugier[41], R.Lauhakangas[16], G.Leder[52], F.Ledroit[15], V.Lefebure[2], L.Leinonen[46], A.Leisos[12], R.Leitner[31], J.Lemonne[2], G.Lenzen[54], V.Lepeltier[20], T.Lesiak[19], M.Lethuillier[41], J.Libby[36], W.Liebig[54], D.Liko[9], A.Lipniacka[46], I.Lippi[37], B.Loerstad[25], J.G.Loken[36], J.H.Lopes[49], J.M.Lopez[42], R.Lopez-Fernandez[15], D.Loukas[12], P.Lutz[41], L.Lyons[36], J.MacNaughton[52], J.R.Mahon[6], A.Maio[22], A.Malek[54], T.G.M.Malmgren[46], S.Maltezos[33], V.Malychev[17], F.Mandl[52], J.Marco[42], R.Marco[42], B.Marechal[49], M.Margoni[37], J-C.Marin[9], C.Mariotti[9], A.Markou[12], C.Martinez-Rivero[20], F.Martinez-Vidal[51], S.Marti i Garcia[9], J.Masik[13], N.Mastroyiannopoulos[12], F.Matorras[42], C.Matteuzzi[29], G.Matthiae[39], F.Mazzucato[37], M.Mazzucato[37], M.Mc Cubbin[23], R.Mc Kay[1], R.Mc Nulty[23], G.Mc Pherson[23], C.Meroni[28], W.T.Meyer[1], E.Migliore[9], L.Mirabito[26], W.A.Mitaroff[52], U.Mjoernmark[25], T.Moa[46], M.Moch[18], R.Moeller[30], K.Moenig[9,11], M.R.Monge[14], X.Moreau[24], P.Morettini[14], G.Morton[36], U.Mueller[54], K.Muenich[54], M.Mulders[32], C.Mulet-Marquis[15], R.Muresan[25], W.J.Murray[38], B.Muryn[15,19], G.Myatt[36], T.Myklebust[34], F.Naraghi[15], M.Nassiakou[12], F.L.Navarria[5], S.Navas[51], K.Nawrocki[53], P.Negri[29], N.Neufeld[9], R.Nicolaidou[41], B.S.Nielsen[30], P.Niezurawski[53], M.Nikolenko[10,17], V.Nomokonov[16], A.Nygren[25], V.Obraztsov[44], A.G.Olshevski[17], A.Onofre[22], R.Orava[16], G.Orazi[10], K.Osterberg[16], A.Ouraou[41], M.Paganoni[29], S.Paiano[5], R.Pain[24], R.Paiva[22], J.Palacios[36], H.Palka[19], Th.D.Papadopoulou[33,9], K.Papageorgiou[12], L.Pape[9], C.Parkes[9], F.Parodi[14], U.Parzefall[23], A.Passeri[40], O.Passon[54], T.Pavel[25], M.Pegoraro[37], L.Peralta[22], M.Pernicka[52], A.Perrotta[5], C.Petridou[48], A.Petrolini[14], H.T.Phillips[38], F.Pierre[41], M.Pimenta[22], E.Piotto[28], T.Podobnik[45], M.E.Pol[6], G.Polok[19], P.Poropat[48], V.Pozdniakov[17], P.Privitera[39], N.Pukhaeva[17], A.Pullia[29], D.Radojicic[36], S.Ragazzi[29], H.Rahmani[33], J.Rames[13], P.N.Ratoff[21], A.L.Read[34], P.Rebecchi[9], N.G.Redaelli[28], M.Regler[52], J.Rehn[18], D.Reid[32], R.Reinhardt[54], P.B.Renton[36], L.K.Resvanis[3], F.Richard[20], J.Ridky[13], G.Rinaudo[47], O.Rohne[34], A.Romero[47], P.Ronchese[37], E.I.Rosenberg[1], P.Rosinsky[7], P.Roudeau[20], T.Rovelli[5], Ch.Royon[41], V.Ruhlmann-Kleider[41], A.Ruiz[42], H.Saarikko[16], Y.Sacquin[41], A.Sadovsky[17], G.Sajot[15], J.Salt[51], D.Sampsonidis[12], M.Sannino[14], Ph.Schwemling[24], B.Schwering[54], U.Schwickerath[18], F.Scuri[48], P.Seager[21], Y.Sedykh[17], A.M.Segar[36], N.Seibert[18], R.Sekulin[38], R.C.Shellard[6], M.Siebel[54], L.Simard[41], F.Simonetto[37], A.N.Sisakian[17], G.Smadja[26], O.Smirnova[25], G.R.Smith[38], A.Sokolov[44], O.Solovianov[44], A.Sopczak[18], R.Sosnowski[53], T.Spassov[22], E.Spiriti[40], S.Squarcia[14], C.Stanescu[40], S.Stanic[45], M.Stanitzki[18], K.Stevenson[36], A.Stocchi[20], J.Strauss[52], R.Strub[10], B.Stugu[4], M.Szczekowski[53], M.Szeptycka[53], T.Tabarelli[29], A.Taffard[23], F.Tegenfeldt[50], F.Terranova[29], J.Thomas[36], J.Timmermans[32], N.Tinti[5], L.G.Tkatchev[17], M.Tobin[23], S.Todorova[10], A.Tomaradze[2], B.Tome[22], A.Tonazzo[9],

L.Tortora[40], P.Tortosa[51], G.Transtromer[25], D.Treille[9], G.Tristram[8], M.Trochimczuk[53], C.Troncon[28], A.Tsirou[9], M-L.Turluer[41], I.A.Tyapkin[17], S.Tzamarias[12], O.Ullaland[9], V.Uvarov[44], G.Valenti[5], E.Vallazza[48], C.Vander Velde[2], P.Van Dam[32], W.Van Den Boeck[2], W.K.Van Doninck[2], J.Van Eldik[32], A.Van Lysebetten[2], N.van Remortel[2], I.Van Vulpen[32], G.Vegni[28], L.Ventura[37], W.Venus[38,9], F.Verbeure[2], M.Verlato[37], L.S.Vertogradov[17], V.Verzi[39], D.Vilanova[41], L.Vitale[48], E.Vlasov[44], A.S.Vodopyanov[17], G.Voulgaris[3], V.Vrba[13], H.Wahlen[54], C.Walck[46], A.J.Washbrook[23], C.Weiser[9], D.Wicke[54], J.H.Wickens[2], G.R.Wilkinson[9], M.Winter[10], M.Witek[19], G.Wolf[9], J.Yi[1], O.Yushchenko[44], A.Zaitsev[44], A.Zalewska[19], P.Zalewski[53], D.Zavrtanik[45], E.Zevgolatakos[12], N.I.Zimin[17,25], A.Zintchenko[17], G.C.Zucchelli[46], G.Zumerle[37]

[1] Department of Physics and Astronomy, Iowa State University, Ames IA 50011-3160, USA
[2] Physics Department, Univ. Instelling Antwerpen, Universiteitsplein 1, B-2610 Antwerpen, Belgium
and IIHE, ULB-VUB, Pleinlaan 2, B-1050 Brussels, Belgium
and Faculté des Sciences, Univ. de l'Etat Mons, Av. Maistriau 19, B-7000 Mons, Belgium
[3] Physics Laboratory, University of Athens, Solonos Str. 104, GR-10680 Athens, Greece
[4] Department of Physics, University of Bergen, Allégaten 55, NO-5007 Bergen, Norway
[5] Dipartimento di Fisica, Università di Bologna and INFN, Via Irnerio 46, IT-40126 Bologna, Italy
[6] Centro Brasileiro de Pesquisas Físicas, rua Xavier Sigaud 150, BR-22290 Rio de Janeiro, Brazil
and Depto. de Física, Pont. Univ. Católica, C.P. 38071 BR-22453 Rio de Janeiro, Brazil
and Inst. de Física, Univ. Estadual do Rio de Janeiro, rua São Francisco Xavier 524, Rio de Janeiro, Brazil
[7] Comenius University, Faculty of Mathematics and Physics, Mlynska Dolina, SK-84215 Bratislava, Slovakia
[8] Collège de France, Lab. de Physique Corpusculaire, IN2P3-CNRS, FR-75231 Paris Cedex 05, France
[9] CERN, CH-1211 Geneva 23, Switzerland
[10] Institut de Recherches Subatomiques, IN2P3 - CNRS/ULP - BP20, FR-67037 Strasbourg Cedex, France
[11] DESY-Zeuthen, Platanenallee 6, D-15735 Zeuthen, Germany
[12] Institute of Nuclear Physics, N.C.S.R. Demokritos, P.O. Box 60228, GR-15310 Athens, Greece
[13] FZU, Inst. of Phys. of the C.A.S. High Energy Physics Division, Na Slovance 2, CZ-180 40, Praha 8, Czech Republic
[14] Dipartimento di Fisica, Università di Genova and INFN, Via Dodecaneso 33, IT-16146 Genova, Italy
[15] Institut des Sciences Nucléaires, IN2P3-CNRS, Université de Grenoble 1, FR-38026 Grenoble Cedex, France
[16] Helsinki Institute of Physics, HIP, P.O. Box 9, FI-00014 Helsinki, Finland
[17] Joint Institute for Nuclear Research, Dubna, Head Post Office, P.O. Box 79, RU-101 000 Moscow, Russian Federation
[18] Institut für Experimentelle Kernphysik, Universität Karlsruhe, Postfach 6980, DE-76128 Karlsruhe, Germany
[19] Institute of Nuclear Physics and University of Mining and Metalurgy, Ul. Kawiory 26a, PL-30055 Krakow, Poland
[20] Université de Paris-Sud, Lab. de l'Accélérateur Linéaire, IN2P3-CNRS, Bât. 200, FR-91405 Orsay Cedex, France
[21] School of Physics and Chemistry, University of Lancaster, Lancaster LA1 4YB, UK
[22] LIP, IST, FCUL - Av. Elias Garcia, 14-1°, PT-1000 Lisboa Codex, Portugal
[23] Department of Physics, University of Liverpool, P.O. Box 147, Liverpool L69 3BX, UK
[24] LPNHE, IN2P3-CNRS, Univ. Paris VI et VII, Tour 33 (RdC), 4 place Jussieu, FR-75252 Paris Cedex 05, France
[25] Department of Physics, University of Lund, Sölvegatan 14, SE-223 63 Lund, Sweden
[26] Université Claude Bernard de Lyon, IPNL, IN2P3-CNRS, FR-69622 Villeurbanne Cedex, France
[27] Univ. d'Aix - Marseille II - CPP, IN2P3-CNRS, FR-13288 Marseille Cedex 09, France
[28] Dipartimento di Fisica, Università di Milano and INFN, Via Celoria 16, IT-20133 Milan, Italy
[29] Università degli Studi di Milano - Bicocca, Via Emanuelli 15, IT-20126 Milan, Italy
[30] Niels Bohr Institute, Blegdamsvej 17, DK-2100 Copenhagen Ø, Denmark
[31] IPNP of MFF, Charles Univ., Areal MFF, V Holesovickach 2, CZ-180 00, Praha 8, Czech Republic
[32] NIKHEF, Postbus 41882, NL-1009 DB Amsterdam, The Netherlands
[33] National Technical University, Physics Department, Zografou Campus, GR-15773 Athens, Greece
[34] Physics Department, University of Oslo, Blindern, NO-1000 Oslo 3, Norway
[35] Dpto. Fisica, Univ. Oviedo, Avda. Calvo Sotelo s/n, ES-33007 Oviedo, Spain
[36] Department of Physics, University of Oxford, Keble Road, Oxford OX1 3RH, UK
[37] Dipartimento di Fisica, Università di Padova and INFN, Via Marzolo 8, IT-35131 Padua, Italy
[38] Rutherford Appleton Laboratory, Chilton, Didcot OX11 OQX, UK
[39] Dipartimento di Fisica, Università di Roma II and INFN, Tor Vergata, IT-00173 Rome, Italy
[40] Dipartimento di Fisica, Università di Roma III and INFN, Via della Vasca Navale 84, IT-00146 Rome, Italy
[41] DAPNIA/Service de Physique des Particules, CEA-Saclay, FR-91191 Gif-sur-Yvette Cedex, France
[42] Instituto de Fisica de Cantabria (CSIC-UC), Avda. los Castros s/n, ES-39006 Santander, Spain
[43] Dipartimento di Fisica, Università degli Studi di Roma La Sapienza, Piazzale Aldo Moro 2, IT-00185 Rome, Italy
[44] Inst. for High Energy Physics, Serpukov P.O. Box 35, Protvino, (Moscow Region), Russian Federation
[45] J. Stefan Institute, Jamova 39, SI-1000 Ljubljana, Slovenia and Laboratory for Astroparticle Physics,
Nova Gorica Polytechnic, Kostanjeviska 16a, SI-5000 Nova Gorica, Slovenia,
and Department of Physics, University of Ljubljana, SI-1000 Ljubljana, Slovenia
[46] Fysikum, Stockholm University, Box 6730, SE-113 85 Stockholm, Sweden
[47] Dipartimento di Fisica Sperimentale, Università di Torino and INFN, Via P. Giuria 1, IT-10125 Turin, Italy
[48] Dipartimento di Fisica, Università di Trieste and INFN, Via A. Valerio 2, IT-34127 Trieste, Italy
and Istituto di Fisica, Università di Udine, IT-33100 Udine, Italy
[49] Univ. Federal do Rio de Janeiro, C.P. 68528 Cidade Univ., Ilha do Fundão BR-21945-970 Rio de Janeiro, Brazil
[50] Department of Radiation Sciences, University of Uppsala, P.O. Box 535, SE-751 21 Uppsala, Sweden
[51] IFIC, Valencia-CSIC, and D.F.A.M.N., U. de Valencia, Avda. Dr. Moliner 50, ES-46100 Burjassot (Valencia), Spain
[52] Institut für Hochenergiephysik, Österr. Akad. d. Wissensch., Nikolsdorfergasse 18, AT-1050 Vienna, Austria
[53] Inst. Nuclear Studies and University of Warsaw, Ul. Hoza 69, PL-00681 Warsaw, Poland
[54] Fachbereich Physik, University of Wuppertal, Postfach 100 127, DE-42097 Wuppertal, Germany

1 Introduction

The differential cross-section for fermion pair production in the process $e^+e^- \to Z \to f\bar{f}$ in first order can be written as :

$$\frac{d\sigma_{f\bar{f}}}{d\cos\theta} = \sigma_{f\bar{f}}^{tot}(s)\left(1+\cos^2\theta+\frac{8}{3}A_{FB}^{f\bar{f}}(s)\cos\theta\right)\frac{3}{8}, \tag{4}$$

where $\sigma_{f\bar{f}}^{tot}$ is the total cross-section, s is the total energy and θ is the angle between the outgoing fermion f and the incoming electron.

The $\cos\theta$ term corresponds to a forward-backward asymmetry $A_{FB}^{f\bar{f}}$ in the fermion production. This asymmetry can be expressed in the Standard Model as a function of the vector v_f and axial vector a_f couplings of the fermion to the Z boson. From the forward-backward asymmetry at the Z the pole asymmetry $A_{f\bar{f}}^0$ can be obtained:

$$A_{f\bar{f}}^0 = \frac{3}{4}A_e A_f = \frac{3}{4}\frac{2v_e a_e}{v_e^2+a_e^2}\frac{2v_f a_f}{v_f^2+a_f^2}, \tag{5}$$

where A_e and A_f are the parity violating couplings of the electron and fermion to the Z. In the improved Born approximation, the higher order radiative corrections can be taken into account by substituting in equations (4) and (5) the effective couplings $\bar{v}_f$ and $\bar{a}_f$. In this way an effective electroweak mixing angle θ_{eff}^{lept} is defined as :

$$\sin^2\theta_{eff}^{lept} = \frac{1}{4|Q_f|}\left(1-\frac{\bar{v}_f}{\bar{a}_f}\right) \tag{6}$$

where Q_f is the fermion electric charge. Therefore the measurement of the forward-backward asymmetry of fermions allows a measurement of the effective electroweak mixing angle and an accurate test of the Standard Model. Several measurements have been already performed by the LEP collaborations for the bottom and the charm quarks [1] :

$$\begin{aligned} A_{b\bar{b}}^0 &= 0.0990 \pm 0.0021 \\ A_{c\bar{c}}^0 &= 0.0709 \pm 0.0044. \end{aligned} \tag{7}$$

From equations (5) and (6) it follows that the down-type quarks are more sensitive than up-type quarks or leptons to the electroweak mixing angle.

The predicted difference $A_{FB}^{b\bar{b}} - A_{FB}^{s\bar{s}}$ is of the order of $\mathcal{O}\,(10^{-4})$ [2], beyond the present experimental accuracy. Thus the measurement of the s quark asymmetry is a universality test of the quark couplings. It further provides a measurement of the effective electroweak mixing angle for strange quarks and a determination of the parity violating coupling of the strange quark to the Z.

The first measurement of $A_{FB}^{s\bar{s}}$ has been presented by the DELPHI collaboration using the data collected in 1992 [3]. More recently a measurement has been provided also by the OPAL collaboration [4]. The present paper gives a precise measurement based on 3.2 M hadronic events collected by DELPHI in 1992-1995. Two alternative analyses are presented, giving consistent results and similar total systematic uncertainties.

The method used to measure $A_{FB}^{s\bar{s}}$ in this analysis is similar to the one used for $A_{FB}^{b\bar{b}}$ which relies on the semileptonic decays of B hadrons. A strange hadron of high momentum is likely to be a signature of a primary s quark. Moreover, the electric charge (for mesons) carries information on the charge of the primary quark produced in the same event hemisphere and thus allows the s quark to be separated from the $\bar{s}$. Identified high energy charged kaons with momentum in the range $10 \le p \le 24$ GeV/c are used to

measure the s quark forward-backward asymmetry with the highest available precision. The fraction of s quarks in hadronic events will not be measured and assumed from the Standard Model.

2 Detector description and event selection

The DELPHI detector has been described in detail elsewhere [5]. Only the components relevant for this analysis are discussed below. The reference frame used has the z axis along the incoming e^- direction, the polar angle θ is defined with respect to this axis and the azimuthal angle ϕ in the $R\phi$ plane orthogonal to this direction.

In the barrel region, the tracking system is composed of cylindrical coaxial detectors, the Vertex Detector (VD), the Inner Detector (ID), the Time Projection Chamber (TPC) and the Outer Detector (OD).

The VD is the nearest detector to the interaction region and consists of 3 concentric layers of silicon micro-strips located at average radii of 6.3 cm, 8.8 cm and 10.9 cm. For polar angles of $44° \leq \theta \leq 136°$, a particle crosses all three layers of the VD. At the start of 1994, the first (Closer) and third (Outer) layers were equipped with double-sided silicon detectors, giving measurements also in the z direction. The polar angle coverage of the Closer layer was increased to $25° \leq \theta \leq 155°$. The ID is a cylindrical drift chamber (inner radius 12 cm and outer radius 22 cm) covering polar angles between 23° and 157°. Since the beginning of 1995 a new longer ID has been operational. Polar angle acceptance is now $15° \leq \theta \leq 175°$. The TPC is the main tracking device of DELPHI, a cylinder of inner radius 30 cm, outer radius 122 cm, 2.7 m long, providing up to 16 measured space points per particle trajectory at radii of 40 to 110 cm between polar angles of $39° \leq \theta \leq 141°$. At least three space points per track are available for polar angles of $20° \leq \theta \leq 160°$. The OD consists of 5 layers of drift cells at radii between 192 cm and 208 cm, covering polar angles between 43° and 137°.

In the forward region ($11° \leq \theta \leq 33°$ and $117° \leq \theta \leq 169°$) the tracking system is completed with two sets of drift chambers placed at $\pm$ 160 cm (FCA) and $\pm$ 270 cm (FCB) in z.

A super-conducting solenoid surrounding the whole tracking system generates a 1.2 T magnetic field coaxial with the beam direction, used for the measurement of the charged particle momenta.

The average momentum resolution depending on the detectors included in the fit, ranges from $\delta p/p^2 \simeq 0.001$ to 0.01 $(\mathrm{GeV/c})^{-1}$.

The particle identification is based on Ring Imaging CHerenkov (RICH) detectors in the barrel and forward regions. The Barrel RICH (BRICH [6]), placed between the TPC and the OD, covers the angular region $40° \leq \theta \leq 140°$. The Forward RICH (FRICH [7]) is located in the end-caps between FCA and FCB covering the polar angles $15° \leq \theta \leq 35°$ and $145° \leq \theta \leq 165°$. The FRICH is used for the data taken in 1994 and 1995. Forward and Barrel RICHes combine two different types of radiators, one liquid and one gaseous, in order to allow π/K/p separation over a large momentum range. In this analysis only the gaseous radiator was used. In the barrel region the gaseous freon C_5F_{12} is used, in the forward region C_4F_{10}. The Cherenkov light cone emitted by a particle in this radiator is focussed on the photosensitive device by parabolic and spherical mirrors, which are subdivided in sets according to polar angle θ ranges. In the BRICH 12 polar angle intervals (corresponding to $0.04 < |\cos\theta| < 0.68$) and 4 for the FRICH (corresponding to $0.82 < |\cos\theta| < 0.94$) were used.

For the analysis, charged particles were accepted if they had :

- a polar angle $20° \leq \theta \leq 160°$;
- a track length in the TPC longer than 30 cm;
- an impact parameter with respect to the interaction point less than 4 cm in the $R\phi$ plane and less than 10 cm in $|z|$;
- a momentum p greater than 0.4 GeV/c with an error $\Delta p/p \leq 1$.

For the calculation of the thrust axis of the event also neutral showers in the calorimeters not associated with charged tracks were used if the reconstructed energy had an error $\Delta E/E \leq 1$. An event was selected as hadronic if :

- the number of selected charged particles was greater than 4;
- the total energy in charged particles was greater than 15 GeV in the whole event and greater than 3 GeV in each event hemisphere as defined by the thrust axis (considering all particles as pions).

A total of 3.2 M hadronic events was selected with these cuts. The residual contamination of $Z \rightarrow \tau\tau$ and $\gamma\gamma$ events was below 0.3%, and the one coming from beam gas interactions below 0.1%. Hadronic events were generated with the JETSET 7.3 model [8], as tuned by the DELPHI Collaboration [9]. The Lund symmetric fragmentation function described the light quark hadronisation process, while the Peterson function was used for the fragmentation of bottom and charm quarks. The detector response was simulated with the DELPHI program DELSIM [10]. A sample of 10.7 M simulated hadronic events was used.

3 Sample selection

The analysis uses the capability of DELPHI to tag individually charged kaons using the RICH detectors. In the barrel and in the forward region, two different analyses have been performed and both use the fast kaon tagging. In the barrel region the fraction of light quark events is enhanced using the b-tagging probability. The contribution from charm and bottom quarks is reduced and the fraction of s quarks is increased. The forward region is relevant for this measurement because the asymmetry is maximal in this region.

The particles identified as kaons are required to lie inside the RICHes and should have momenta between 10 GeV/c and 24 GeV/c. The lower momentum limit is constrained by the Cherenkov emission threshold ($p \sim 8.5$ GeV/c) in the gas radiators of both RICHes. The upper limit is set in order to have a one sigma standard deviation between pions and kaons. If more than one kaon with such characteristics was found in the event, the kaon with highest momentum was considered.

For the barrel analysis, only selected hadronic events with the polar angle of the thrust axis in the range $|\cos\theta_{thrust}| \leq 0.7$ are considered. For the forward analysis, the allowed angular region for the thrust axis is set to $0.8 \leq |\cos\theta_{thrust}| \leq 0.95$. For both analyses a selection of runs was made to select the periods where the gas RICH was fully operational.

The quark direction is estimated using the thrust axis.

3.1 Kaon identification

The kaon identification method is based on the average Cherenkov angle for a reconstructed ring. The Cherenkov angle, the number of photons and the expected error per ring are estimated by a clustering algorithm described in reference [11]. The starting

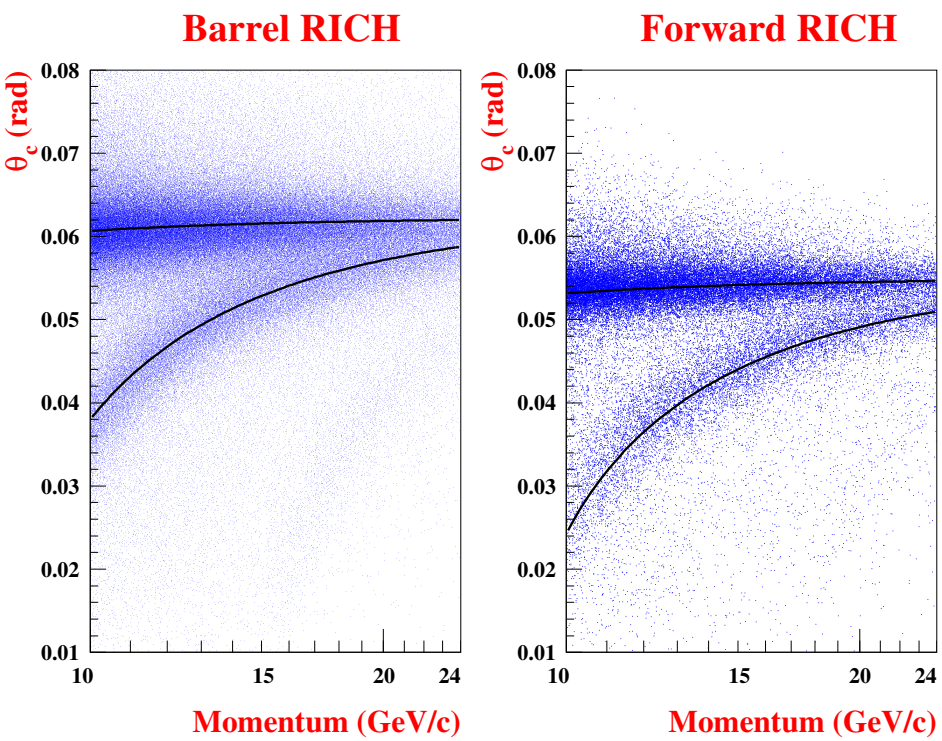

Figure 1: For the 1994 data the reconstructed average Cherenkov angle in the gaseous radiator of (left) the BRICH and (right) the FRICH as a function of the particle momentum ($10 < p < 24$ GeV/c). The two solid lines show the Cherenkov angle for the pion and kaon hypothesis.

point of the clustering procedure is a set of detected single photoelectrons i characterised by a Cherenkov angle (θ_i) and its estimated error (σ_{θ_i}). The photoelectrons are grouped to form clusters in order to reject backgrounds from feedback photons, photons produced by other charged particles, track ionization and other sources [12]. The cluster with the highest number of photoelectrons is chosen and the mean Cherenkov angle θ_c and its expected error σ_{ring} are computed. Based on this information kaons can by identified on a track-by-track basis. The reconstructed average Cherenkov angle in the gaseous radiator of the BRICH and the FRICH as a function of the particle momentum is shown in Figure 1. The curves show a different saturation angle because of the different gases used in the barrel and forward RICHes.

A particle had to pass the track selection criteria given in section 2 and to lie in the RICH acceptance defined in section 3 with a momentum between 10 and 24 GeV/c.

Then a kaon candidate had to satisfy the following criteria:

- only tracks in which the OD or FCB were used in the track fit were selected. This ensures that only well reconstructed particles crossing the RICHes were used ;
- the mean Cherenkov angle was measured if at least 2 photoelectrons were used in the ring ;
- a particle was identified as a kaon if the following conditions on the measured and the expected Cherenkov angles were satisfied:

$$\frac{|\theta_c - \theta_c^K|}{\sigma_{ring}} < 2.5$$
$$\frac{|\theta_c - \theta_c^\pi|}{\sigma_{ring}} > 2$$

  where θ_c^K, θ_c^π are the theoretical expectation for the K and π hypothesis for a given momentum.

In the forward region, an additional cut on the polar angle of the particle was applied for rings in the odd-numbered chambers. Each Forward RICH sector covering 30° azimuthal angle has one odd- and one even-numbered chamber. The chambers can be distinguished by the direction of the drift field. It was found that for odd-numbered chambers in the region $0.82 < |\cos\theta| < 0.87$ the full Cherenkov ring could not be reconstructed, due to the fact that the electrons drift under a Lorentz angle. This zone was removed because it was found that the acceptance was different for positively and negatively charged particles. For even chambers no dead zone within the considered acceptance is present. About 20% of the particles were lost with this cut.

The selected $K^\pm$ had an average identification efficiency of 53% in the Barrel region and 42% in the Forward region according to the simulation. Figures 2 and 3 demonstrate that the behaviour of the particle identification algorithm in the gas radiators of the Barrel and Forward RICH is fairly well reproduced by the simulation. The discrepancies are corrected for in the analysis.

3.2 Light quark tagging

The selection of events with a true high momentum $K^\pm$ as described in the previous section selected events with an s quark purity of 43% as estimated from the simulation. To improve the s quark fraction in the barrel region ($|\cos\theta_{thrust}| \leq 0.7$), bottom and charm quarks were rejected by using the b-tagging information based on the microvertex detector. This increased the s quark fraction from 43% to 55%. By removing the bottom

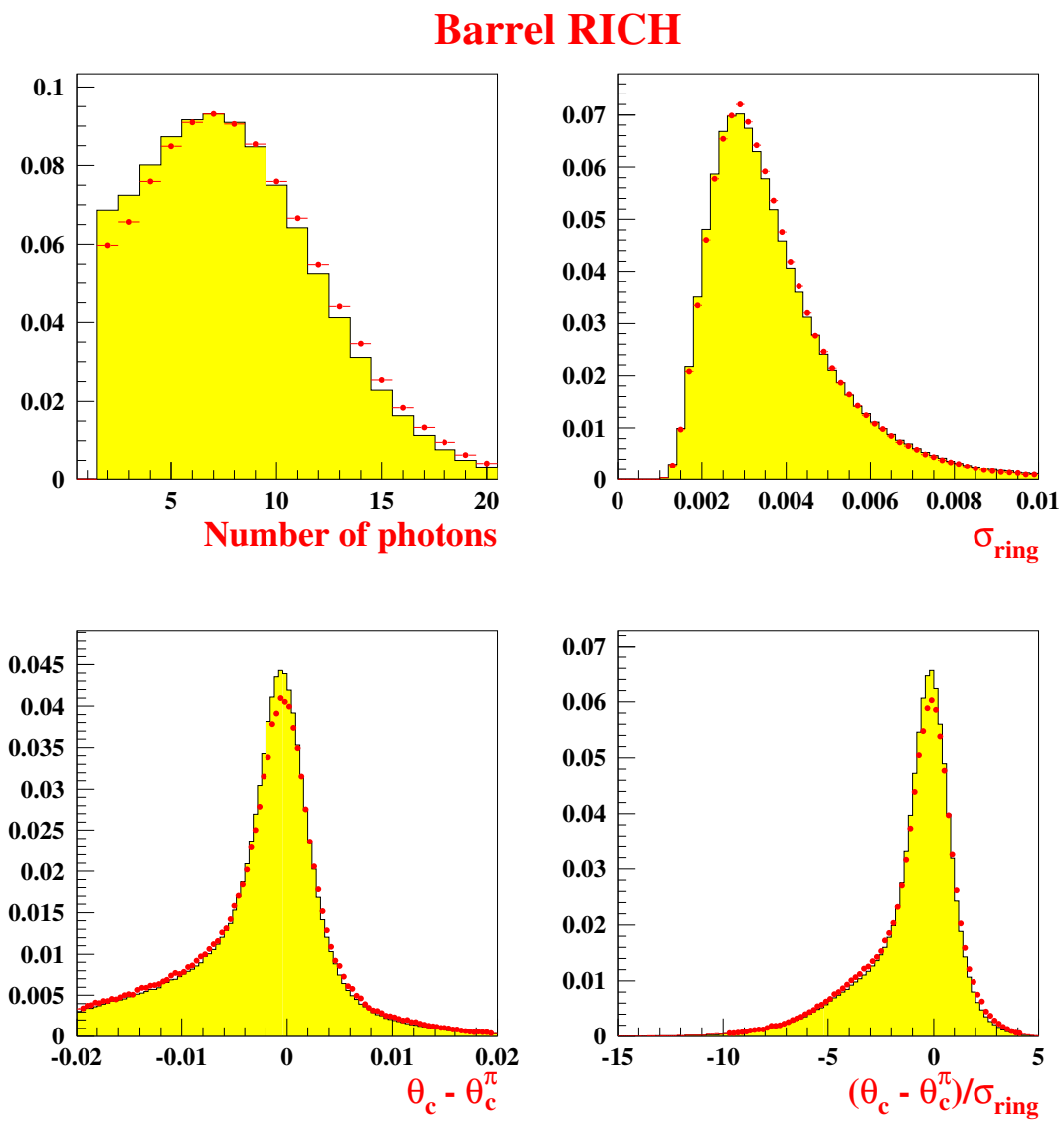

Figure 2: Distributions for charged particles (with momentum between 10 GeV/c and 24 GeV/c) in the gas radiator of the Barrel RICH for 1994 data (dots) and simulation (histograms) for the observed number of photons, the expected error per ring, the difference between the measured Cherenkov angle and the expected one in the pion hypothesis, and the pull for the pion hypothesis.

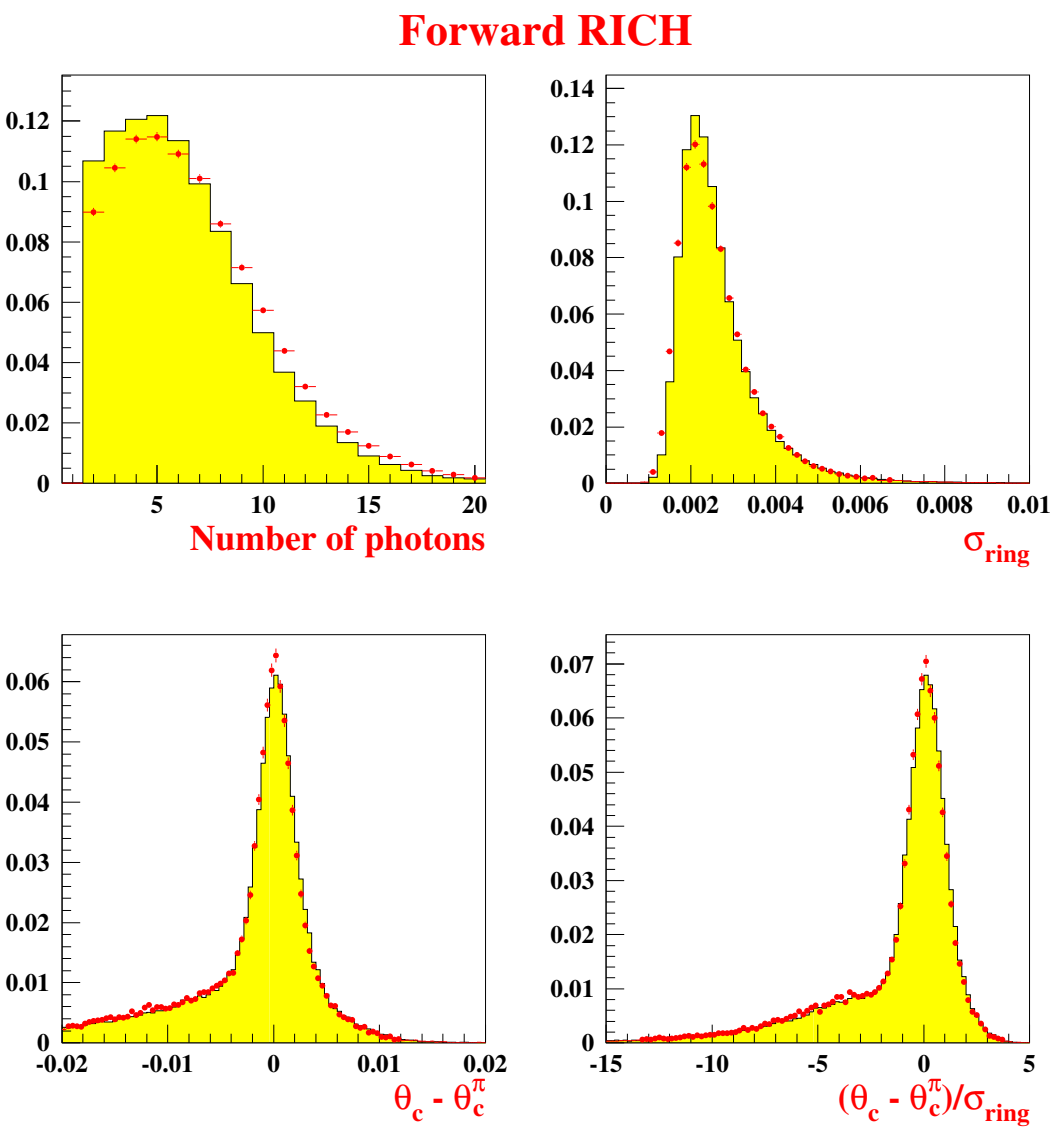

Figure 3: Same as Figure 2 for the Forward RICH.

and charm quarks, the measurement becomes less sensitive to the systematic uncertainties in the kaon production rates and spectra in the decay of heavy quarks. In the forward region this selection cannot be applied because the FRICH has little overlap with the acceptance of the microvertex detector.

The b-tagging algorithm is based on the precise measurement of the impact parameters with the microvertex detector [13]. This quantity is defined as the minimum distance between the charged particle trajectory and the reconstructed primary vertex. It is positive if the intersection of the track with its jet axis is in front of the primary vertex. The ratio of the impact parameter and of its error, called significance (S), is used because it is sensitive to the lifetime. Hadrons containing heavy quarks have a relatively long lifetime and large masses. These two characteristics of B hadrons imply that their decay products will have large impact parameter with respect to the primary vertex.

The negative part of the significance distribution is only sensitive to detector resolution effects and not to secondary decays, and it is therefore used to compute, from data themselves, a significance probability density for tracks coming from the primary vertex. The probabilities for selected tracks in a given sample can be combined to compute the global probability that this sample of tracks is coming from the primary vertex. This probability has a flat distribution for tracks coming from the primary vertex by construction, while it is peaked at small values for tracks coming from secondary decay vertices.

The discriminant variable used to reject events from heavy quarks is the probability P_E^+ computed on a event-by-event basis for all the tracks with hits in the VD and positive measured significance. All the events with $P_E^+ > 0.15$ were accepted. The cut value was chosen as a compromise between decreasing as much as possible the charm contamination and keeping the s tagging efficiency above 80%. The bottom quark contribution is below 1%.

4 Charged kaon asymmetry

4.1 Experimental procedure

In order to measure $A^0_{s\bar{s}}$, the asymmetry of the number of selected events with negative and positive charged kaons was evaluated. This asymmetry A^K_{FB}, which will be referred to hereafter as the charged kaon asymmetry, can be written as a linear combination of the quark forward-backward asymmetries:

$$A^K_{FB} = \sum_q \alpha_q (2c_q - 1) A_{q\bar{q}} \qquad (q = \mathrm{d, u, s, c, b}). \tag{8}$$

The α_q coefficients are the fractions of selected events with primary quark q, while c_q are the probabilities that the kaon charge corresponds to the charge of the primary quark. E.g. a K^- in a given hemisphere correctly tags a primary s quark. In this section the measurement of A^K_{FB} is discussed, while the details of the extraction of $A^0_{s\bar{s}}$ are described in the next section.

The measurement of A^K_{FB} assumes the theoretical behaviour of the asymmetry as a function of the quark polar angle θ to be valid :

$$A^K(\cos\theta) = \frac{8}{3} A^K_{FB} \frac{\cos\theta}{1+\cos^2\theta} \tag{9}$$

and uses as estimator of the quark polar angle the thrust axis polar angle θ_{thrust}, orienting the axis parallel (anti-parallel) to the $\mathrm{K^-}$ ($\mathrm{K^+}$) projection along the axis itself. The

asymmetry:

$$A_i^K = \frac{N_{K^-} - N_{K^+}}{N_{K^-} + N_{K^+}} \tag{10}$$

between the number of events with K^- and K^+ falling in a given angular interval i is measured and a fit of the distribution of the A_i^K to the theoretical distribution (9) is done in order to extract A_{FB}^K. Because positive and negative charged kaons are compared per bin of $\cos\theta$, possible differences in the acceptance for the forward and backward hemispheres cancel.

A binned χ^2 fit is used to extract A_{FB}^K. The measured forward-backward asymmetry A_i^K has to be corrected for the purity of the sample (due to misidentified pions) and the asymmetry due to the different cross-sections for interactions of K^- and K^+ with the detector material. Both corrections depend on the $K^\pm$ polar angle. For this reason the asymmetry A_i^K is evaluated in bins of the polar angle of the kaon θ_K; the bins are chosen such that the corrections needed vary only slightly inside the bin, and therefore an average value can be safely used for all the events in the given bin. The natural choice for the bin is a RICH mirror. For a given bin i with n_i events one has to estimate the weight w_i according to (9):

$$w_i = \frac{8}{3}\frac{1}{n_i}\sum_{j=1}^{n_i}\frac{\cos\theta_j}{1+\cos^2\theta_j}, \tag{11}$$

where θ_j is the thrust axis polar angle in the j-th event with a $K^\pm$ falling in the bin i. For a given A_{FB}^K, the observed asymmetry for a bin i in $\cos\theta_K$, corrected for the K purity and the effects of interactions with the material, can be expressed as:

$$A_i^{obs} = w_i A_{FB}^K \tag{12}$$

If the purity equals 1 and the asymmetry from interactions with the material is zero, the A_i^{obs} is simply equal to the kaon asymmetry in bin i A_i^K (10). The corrections which relate A_i^{obs} in the θ_K bin to the measured kaon asymmetry A_i^K are expressed by the following equations :

$$A_i^{obs} = \frac{(1-r_i) + A_i^{corr}(1+r_i)}{(1+r_i) + A_i^{corr}(1-r_i)} \simeq A_i^{corr} + \frac{1}{2}(1-r_i) \tag{13}$$

$$A_i^{corr} = \frac{A_i^K - (1-P_i)A^{bckg}}{P_i}, \tag{14}$$

where P_i is the purity of the kaon sample for a given $\cos\theta_K$ bin. The different cross-section of K^- and K^+ with the detector material is expressed as the ratio $r_i = \epsilon_{K^-}/\epsilon_{K^+}$ for a given θ_K bin, where ϵ is the probability for a K of a given charge to reach the OD (in the barrel region) or the FCB (in the forward region) without interacting with the detector material. The asymmetry from interactions with the material A_i^{mat} is defined as $\frac{1}{2}(1-r_i)$, and is described in more detail in subsection 4.1.1.

A^{bckg} is the asymmetry for the misidentified particles, averaged over all quarks:

$$A^{bckg} = \sum_q \alpha_q^{bckg}(2c_q^{bckg} - 1)A_{q\bar{q}} \qquad q = \mathrm{d,u,s,c,b}, \tag{15}$$

where α_q^{bckg} is the fraction of $q\bar{q}$ events with a misidentified K, c_q^{bckg} is the probability that the primary quark charge is correctly tagged by the misidentified K and $A_{q\bar{q}}$ are the quark asymmetries. A^{bckg} is computed directly with the full detector simulation. The

$\sqrt{s}$ (GeV)	A^{bckg}	
	Barrel	Forward
89.5	0.0104	0.0122
91.2	0.0020	0.0046
93.0	−0.0037	−0.0056
syst.error	0.0016	0.0030

Table 1: The background asymmetry for different centre-of-mass energy and the systematic error on it.

dominant background is due to misidentified pions. In order to reduce the statistical error on A^{bckg}, tracks identified as pions in the RICHes were used. The pion momentum spectrum was reweighted to obtain the spectrum of misidentified kaons. The coefficients α_q^{bckg} and c_q^{bckg} were computed in this way, and all the quark asymmetries were fixed at the Standard Model values as predicted by ZFITTER [14] with $M_{\rm Z} = 91.1866$ GeV/c^2, $m_t = 173$ GeV/c^2, $m_H = 115$ GeV/c^2, $\alpha_s = 0.122$ as input parameters. The background asymmetries computed for different centre-of-mass energy have negligible systematical errors with respect to statistical ones. The systematic error on A^{bckg} is obtained by recalculating the α_q and c_q coefficients by changing the relevant simulation parameters (listed in Table 10) for charm, bottom and light quark events. The results are summarised in Table 1.

The experimental charged kaon asymmetry A_{FB}^K in the barrel or forward is finally extracted from the minimization of the χ^2 function :

$$\chi^2 \;=\; \sum_{i=1}^{m} \left(\frac{w_i A_{FB}^K - A_i^{obs}}{\sigma_i} \right)^2 , \tag{16}$$

where w_i are the weights defined above, σ_i is the statistical error on the asymmetry A_i^{obs}, and i runs over the m bins in $\cos\theta_{\rm K}$, 12 for the Barrel region and 4 for the Forward one.

4.1.1 Asymmetry from interactions in the detector material

The asymmetry from interactions with the material A_i^{mat} is in first approximation proportional to the material length crossed, which has a $(1/\sin\theta_{\rm K})$ angular dependence on the kaon polar angle in the barrel region. In order to obtain a small statistical uncertainty on the material asymmetry, a fast analytical calculation was done using the DELPHI materials database and the nuclear interaction cross-sections for a grid of points in the 3-dimensional space of K momenta, polar and azimuthal angles, and a weighted mean according to the distributions of these three variables was computed for every mirror. The statistical error in this procedure was negligible. The systematic uncertainty was found to be 0.0015 averaged over the polar angular range.

A second technique is used to extract the asymmetry from interactions with the material for charged kaons from the 2.4 M simulated hadronic events. A fit was done to the distribution of the asymmetry versus the number of stopped kaons as a function of the polar angle. It can be shown that the asymmetry versus the number of stopped charged kaons follows a power law. From the fitted function a more precise estimate of the asymmetry was obtained. The asymmetry from interaction with the material as a function of the cosine of the polar angle is shown in Figure 4; it ranges from 2% to 0.7% for increasing θ. The systematic error on the asymmetry is 10%, mainly coming from

uncertainties in the difference in the nuclear cross-sections of p(n)K^+ and p(n)K^-. The two methods give the consistent results and agree to better than 0.0015. The effect on the kaon forward-backward asymmetry is very small due to the fact that the asymmetry is symmetric in $\cos\theta$.

4.1.2 Purity evaluation

The kaon purity, defined as the fraction of kaons in the tagged kaon sample, is obtained from the full DELPHI simulation. It is mainly a function of the kaon polar angle. The distribution for the corrected purity is shown in Figure 4 (plot on the right). On average it is 80% in the barrel region and 74% in the forward region, almost constant in the whole momentum window. The misidentified particles are mainly pions and only 20% are protons.

Extensive checks were made of the purity evaluation. Real and simulated data were

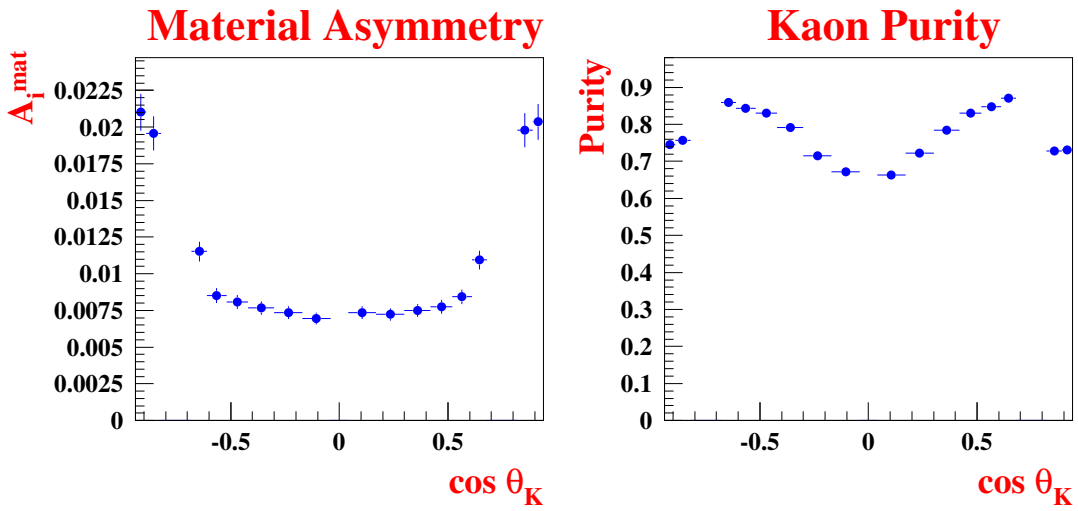

Figure 4: The asymmetry from interactions with the material ($A_i^{mat} = \frac{1}{2}(1 - r_i)$) (left plot) for the 1994 data and the charged kaon purity (right plot) in the momentum range $10 < p < 24$ GeV/c in both RICHes as a function of the $\cos\theta$ of the kaon.

compared in detail for the number of photons, the error per ring, the mean Cherenkov angle w.r.t. the pion hypothesis and the pull distribution for the pion hypothesis (see Figures 2 and 3 for the 1994 data) and good agreement was found for both RICHes. Some residual discrepancies can be seen in these distributions. This suggests correcting the simulated efficiency to identify a $\pi^\pm$ as a $K^\pm$, hereafter called $\pi^\pm$ misidentification probability, and therefore the fraction of pions in the tagged kaon sample.

Two complementary approaches were followed. In the barrel region the samples of high purity muons and of pions identified in the TPC were used to compare the misidentification efficiency in real and simulated data for tracks with momenta between 10 and 24 GeV/c. The results for different years are shown in Table 2. Muons were tagged with the muon chambers and the ionization energy loss measured in the TPC was used to remove kaons in this sample. The residual kaon contamination estimated from simulation was

Year	1992		1993	
	Data	Monte Carlo	Data	Monte Carlo
π sample	10598	84791	9685	86651
$\pi \to K$	575	3177	468	3309
Prob($\pi \to K$) %	5.42 $\pm$ 0.23	3.75 $\pm$ 0.07	4.83 $\pm$ 0.23	3.82 $\pm$ 0.07
ratio Data/Simulation	1.45 ± 0.07		1.26 ± 0.06	
μ sample	781	5862	734	6074
$\mu \to K$	18	110	13	107
Prob($\mu \to K$) %	2.30 $\pm$ 0.55	1.88 $\pm$ 0.18	1.77 $\pm$ 0.50	1.76 $\pm$ 0.17
ratio Data/Simulation	1.22 ± 0.32		1.0 ± 0.3	

Year	1994		1995	
	Data	Monte Carlo	Data	Monte Carlo
π sample	48570	281258	20783	60071
$\pi \to K$	2641	11182	1082	2509
Prob($\pi \to K$) %	5.44 $\pm$ 0.11	3.98 $\pm$ 0.04	5.21 $\pm$ 0.16	4.18 $\pm$ 0.09
ratio Data/Simulation	1.37 ± 0.03		1.25 ± 0.05	
μ sample	3623	21521	1517	4381
$\mu \to K$	116	413	48	104
Prob($\mu \to K$) %	3.20 $\pm$ 0.30	1.92 $\pm$ 0.10	3.16 $\pm$ 0.46	2.37 $\pm$ 0.24
ratio Data/Simulation	1.67 ± 0.18		1.33 ± 0.24	

Table 2: Comparison of the Data and Simulation on the misidentification rate in the barrel RICH for pion and muon samples.

0.35% in the muon and 2.0% in the pion samples. Due to the very high $\pi^{\pm}/\mu$ rejection power of the RICH, the statistics left after kaon identification in the μ sample was very small and no momentum or angular dependence of the correction to the μ misidentification efficiency could be studied. The results for the muon samples give an average ratio of misidentification efficiencies in real and simulated data of 1.41 ± 0.12(stat.) with a systematic error of 10%. After kaon identification, the kaon contamination estimated from simulation in the remaining $\pi^{\pm}$ sample was of 25% and only a rough estimation of the $\pi^{\pm}$ misidentification efficiency could be made. The results for the pion samples led to the average ratio of 1.34 ± 0.02(stat.) with a systematic uncertainty of 20%. The results (see Table 2) found in the pion and muon samples are in agreement and compatible for the different years.

The second method that was finally used to evaluate and correct the purity is based on the mean Cherenkov angle distribution. The Cherenkov angle distribution has two components: one Gaussian component centered around the expected Cherenkov angle for a given particle hypothesis and one background term which is approximately linear in the Cherenkov angle. Particles can be misidentified because a separation of only two standard deviations from the pion hypothesis is required, or because of the presence of background. To study these effects, particles outside the pion and kaon signal regions were selected in real and simulated data. Two regions were defined where the number of particles were counted in real data and simulation :

$$A : \frac{\theta_c - \theta_c^{\pi}}{\sigma_{ring}} > 2.5$$

$$B : \frac{\theta_c - \theta_c^{K}}{\sigma_{ring}} > 2.5 \text{ and } \frac{\theta_c - \theta_c^{\pi}}{\sigma_{ring}} < -2.5.$$

It was found that for the 1992-5 data an average scaling factor of 1.4 ± 0.1 in the barrel region, and 1.05 ± 0.1 in the forward region, should be applied to the simulated data.

The scaling factors are similar for regions A and B. The scaling factor for pions and muons in the barrel in Table 2 is compatible with this result. A small simulation program was written to understand these scaling factors in terms of the background rate. An increase in the linear background term can explain the observed scaling factors. After scaling up the background, the purities extracted from simulated data were decreased by between 0.4% and 4.9% as a function of the polar angle (the correction term decreases when $|\cos\theta_K|$ increases); the purity corrected in this way is shown in Figure 4. With the simulation program the effect of a shift in the mean Cherenkov angle w.r.t. the simulation data and discrepancies in the expected error per ring were propagated. The Cherenkov angle can be shifted at most by 0.25 mrad and the resolution per ring is at most 5% larger than in the simulated data.

The purity was evaluated for each data set. The total associated systematic error on the purity due to the background, Cherenkov angle shift and ring resolution is 1%.

4.2 Results for the on-peak measurements

In the barrel region, 73329 events were selected and used to compute the charged kaon forward-backward asymmetry.

Year	Barrel		Forward	
	# events	A_{FB}^K	# events	A_{FB}^K
1992	10171	0.032 ± 0.013	—	
1993	4948	0.002 ± 0.019	—	
1994	43523	0.0450 ± 0.0063	9342	0.031 ± 0.011
1995	14687	0.047 ± 0.011	4151	0.058 ± 0.015
1992-5	73329	0.0405 ± 0.0049	13493	0.039 ± 0.009

Table 3: The measurements of A_{FB}^K at 91.2 GeV for the 1992-1995 data. The errors are statistical.

$\sqrt{s}$ (GeV)	Year	Barrel		Forward	
		# events	A_{FB}^K	# events	A_{FB}^K
89.5	1993	1981	0.023 ± 0.029	—	
	1995	2305	0.028 ± 0.028	719	-0.005 ± 0.037
	1993,5	4286	0.025 ± 0.020	719	-0.005 ± 0.037
93.0	1993	3020	0.010 ± 0.024	—	
	1995	3362	0.067 ± 0.023	1193	0.044 ± 0.029
	1993,5	6382	0.040 ± 0.017	1193	0.044 ± 0.029

Table 4: The measurements of A_{FB}^K at 89.5 GeV and 93.0 GeV for the 1993 and 1995 data. The errors are statistical.

The results of the fit minimizing the χ^2 function (16) are summarised in Table 3.

As a consistency check the asymmetries were fitted separately for each detector side, giving the compatible results:

$$A_{FB}^K(z>0) = 0.0421 \pm 0.0068\,(\text{stat.}) \quad (17)$$
$$A_{FB}^K(z<0) = 0.0387 \pm 0.0070\,(\text{stat.}). \quad (18)$$

In the forward region, 13493 events were selected and the results are summarised in Table 3. The results are compatible for the different years.

4.3 Results for the off-peak measurements

The statistics and results of the fit for the off-peak measurements are listed in Table 4.

The contributions to the experimental uncertainty on the A_{FB}^K, coming from the sources discussed in section 4.1, are the same for on and off peak measurements and are listed in Table 5. The results are compatible for the different years.

5 s quark asymmetry

5.1 Procedure

The s quark Born asymmetry $A_{s\bar{s}}^0$ can be extracted from the charged kaon asymmetry using the expression (8). The α_q coefficients are the fractions of selected events with

Contributions to the systematic error on A_{FB}^{K} ($\times 10^{-4}$)	Barrel	Forward
Kaon purity	1.3	2.5
K^+/K^- interactions with material	0.2	0.7
A^{bckg}	4.6	8.2
Total	4.8	8.6

Table 5: Contributions to the systematic uncertainty on the charged kaon asymmetries in the Barrel and in the Forward regions.

Flavour	Barrel		Forward	
	α_q	c_q	α_q	c_q
d	0.1425 ± 0.0013	0.328 ± 0.004	0.1038 ± 0.0021	0.329 ± 0.009
u	0.1356 ± 0.0012	0.264 ± 0.004	0.0979 ± 0.0020	0.246 ± 0.009
s	0.5523 ± 0.0029	0.868 ± 0.002	0.4290 ± 0.0048	0.878 ± 0.003
c	0.1600 ± 0.0013	0.835 ± 0.003	0.2331 ± 0.0033	0.859 ± 0.005
b	0.0091 ± 0.0003	0.809 ± 0.013	0.1359 ± 0.0024	0.809 ± 0.007

Table 6: Computed values for the flavour selected fractions (α_q) and quark charge identification efficiencies (c_q) for the Barrel and the Forward regions in 1994. The errors given are due to the limited simulated statistics.

primary quark q, and can be expressed in terms of the original fraction of a flavour in a hadronic sample $R_q = \Gamma_q/\Gamma_{had}$ and the flavour tagging efficiency ϵ_q as :

$$\alpha_q = \frac{R_q \epsilon_q}{\sum_{f=d,u,s,c,b} R_f \epsilon_f} \quad . \tag{19}$$

The c_q coefficients are the probabilities that the kaon charge corresponds to the charge of the primary quark after the QCD parton cascade. With this definition it is possible to restrict the corrections coming from the perturbative QCD phase of the hadronisation only to the primary quark direction estimator. The values of R_q were computed with ZFITTER while the ϵ_q and the c_q coefficients were evaluated with JETSET PS 7.3 and the full DELPHI simulation. The values are given in Table 6.

The forward-backward asymmetries, $A_{q\bar{q}}$, of equation (8) can be written in terms of pole asymmetries $A^0_{q\bar{q}}$, and thus in terms of $\sin^2\theta^{lept}_{eff}$ through formulae (5) and (6), according to the following expression:

$$A_{q\bar{q}} \;=\; (A^0_{q\bar{q}} - \sum_i (\delta A_{q\bar{q}})_i)(1 + C_q^{thrust}). \tag{20}$$

The $(\delta A_{q\bar{q}})_i$ terms take into account the effect on the asymmetry due to QED radiative corrections coming from photon emission, the fact that the asymmetry has been measured at $\sqrt{s} \neq M_Z$ and the $\gamma, \gamma Z$ terms in the Born expression. All these coefficients were computed with ZFITTER as was done in [1].

The C_q^{thrust} are coefficients which take into account the fact that the estimated quark direction using the thrust axis differs from the true one because of QCD gluon emission, hadronisation and decays, and experimental reconstruction problems of the thrust axis (undetected particles, charged particle momenta and neutral particle showers energy resolution). These coefficients were computed according to the procedure described in [16]

Flavour	C_q^{thrust}	
	Barrel	Forward
d	-0.029 ± 0.006	-0.013 ± 0.004
u	-0.029 ± 0.006	-0.018 ± 0.005
s	-0.025 ± 0.003	-0.012 ± 0.002
c	-0.020 ± 0.005	-0.011 ± 0.003
b	-0.035 ± 0.015	-0.005 ± 0.002

Table 7: Correction coefficients for bias on primary quark direction due to QCD gluon emission, fragmentation and thrust axis reconstruction when the thrust axis direction is used as an estimator.

using JETSET PS 7.3 and the full detector simulation :

$$C_q^{thrust} = \frac{\sum_f \left(\frac{\cos(\theta^i)}{1+\cos^2(\theta^i)} - \frac{\cos(\theta^f)}{1+\cos^2(\theta^f)} \right)}{\sum_f \frac{\cos(\theta^f)}{1+\cos^2(\theta^f)}}, \tag{21}$$

where θ^i is the initial state quark polar angle and θ^f the final estimate of this angle: e.g. the polar angle of the thrust axis oriented in the hemisphere in which the quark falls after the QCD cascade (in the parton shower approximation). The C_q^{thrust} values are given in Table 7.

The QCD corrections to the forward-backward asymmetries, $A_{q\bar{q}}$, depend strongly on the experimental analysis. For this reason the measured asymmetries are corrected for QCD effects but not for the $(\delta A_{q\bar{q}})_i$ terms at all centre-of-mass energies. Only the s quark pole asymmetry $A^0_{s\bar{s}}$ is corrected for this.

In order to compute $A^0_{s\bar{s}}$ the c and b pole asymmetries were fixed to their own measured values given in (7) while the u and d pole asymmetries were fixed to the Standard Model values $A^0_{d\bar{d}}$=0.1031 and $A^0_{u\bar{u}}$=0.0736. The determination of $A^{s\bar{s}}_{FB}$ depends on the value assumed for the strange quark suppression factor. A value γ_s=0.307 is used in the DELPHI JETSET simulation; it should be noticed however that tuning γ_s in JETSET using the K^0 or the $K^{\pm}$ momentum spectra gives inconsistent results [9]. The s quark pole asymmetries in this analysis were evaluated using a more recent value of 0.285 for γ_s [17]; the systematic error accounts for this shift [9]. The change in the calculated s quark asymmetry can be parametrized as $\Delta A^0_{s\bar{s}} = 0.17\ \Delta\gamma_s$ in the γ_s region between 0.25 and 0.35.

The results for the s quark pole asymmetry for γ_s=0.285 are summarized in Table 8, they are compatible for the different years.

In order to obtain the strange quark forward-backward asymmetries for the off and on peak points we used the predicted asymmetries from the Standard Model for the off and on peak points for the up, down, charm and bottom quarks. The results are summarised in Table 9.

5.2 Systematic errors

Several sources of systematic uncertainties were taken into account. A detailed breakdown of all the error sources to be discussed below and of their own effect on $A^0_{s\bar{s}}$ is given in Table 10. The systematics on the asymmetries evaluated in the Barrel and Forward regions are different due to the different event selection used: the rejection of heavy quarks

Year	$A^0_{s\bar{s}}$	
	Barrel	Forward
1992	0.081 ± 0.033	—
1993	0.007 ± 0.048	—
1994	0.115 ± 0.016	0.058 ± 0.034
1995	0.120 ± 0.028	0.140 ± 0.050
1992-5	0.104 ± 0.012	0.084 ± 0.028

Table 8: Summary of the determination of $A^0_{s\bar{s}}$ for the 1992-1995 data. The errors are statistical only.

$\sqrt{s}$ (GeV)	$A^{s\bar{s}}_{FB}$	
	Barrel	Forward
89.5	0.073 ± 0.051	-0.013 ± 0.119
91.2	0.102 ± 0.012	0.081 ± 0.028
93.0	0.095 ± 0.043	0.065 ± 0.092

Table 9: Summary of the determination of $A^{s\bar{s}}_{FB}$ for the 1992-1995 data. The errors are statistical only.

in the barrel region substantially reduces the systematic error coming from charm and bottom quarks.

- The uncertainties for the charm and bottom forward-backward asymmetries (7) are propagated, taking into account the 10% correlation between these two quantities.
- A source of experimental systematic errors comes from the systematic error on the kaon asymmetry A^K_{FB} listed in Table 5.
- The effect on s-asymmetry from the finite momentum resolution of the K is computed with the full DELPHI simulation, selecting events according to the true momentum of the K instead of the reconstructed one.
- The rest of the uncertainties come from the Monte Carlo modelling. They can be split into four classes: (1) systematic uncertainties from the charm quark, (2) bottom quark and (3) light quark fragmentation, and (4) from the light quark tag in the barrel region.

(1) For charm quarks the following quantities were taken into account: the fractions of different charmed hadrons $f(\mathrm{D}^{\pm})$, $f(\mathrm{D_s})$, $f(\mathrm{D}^0)$, $f(c_{bar})$; the c hadron decay multiplicity; the mean energy taken by the charmed particle $< x_c >$. The uncertainties in these quantities were taken from [16]. Another source of error comes from the uncertainties in the branching ratios of charmed particles into kaons $\mathrm{BR}(\mathrm{D}^0 \to \mathrm{K}^-\mathrm{X})$, $\mathrm{BR}(\mathrm{D}^0 \to \mathrm{K}^+\mathrm{X})$, $\mathrm{BR}(\mathrm{D}^+ \to \mathrm{K}^-\mathrm{X})$, $\mathrm{BR}(\mathrm{D}^+ \to \mathrm{K}^+\mathrm{X})$, $\mathrm{BR}(\mathrm{D_s} \to \mathrm{K}^-\mathrm{X})$, $\mathrm{BR}(\mathrm{D_s} \to \mathrm{K}^+\mathrm{X})$: the values quoted in [15] were used. The simulated events were reweighted according to the uncertainties in all the observables listed, and the variations in $A^0_{s\bar{s}}$ due to the variations in the coefficients α_q and c_q were used to estimate the systematic errors.

(2) For bottom quarks the following quantities were taken into account: the fractions of different beauty hadrons $f(\mathrm{B}^{\pm})$, $f(\mathrm{B_s})$, $f(\mathrm{B}^0)$, $f(b_{bar})$; the b hadron decay multiplicity; the mean energy taken by the beauty particle $< x_b >$. The uncertainties in these quanti-

ties were taken from [16] and [15]. Another source of error comes from the uncertainties in the branching ratios of beauty particles into kaons BR($B^0 \to K^-X$), BR($B^0 \to K^+X$), BR($B^+ \to K^-X$), BR($B^+ \to K^+X$): the values quoted in [18] were used. In addition, the uncertainty in the branching ratio of bottom quarks into kaons BR($b \to K^{\pm}X$) [15] is propagated. Moreover two additional sources of uncertainties were taken into consideration: in events with D_s coming from B_s, the error on the branching ratios of D_s decays into $K^{\pm}$ were considered and the uncertainty in B_d mixing parameter [15]. To obtain the systematic errors the same reweighting procedure is applied.

(3) The parameters describing the fragmentation process of up, down and strange quarks were studied using the JETSET 7.3 PS parameters as they were obtained by a tuning procedure based on LEP data described in [9]. The JETSET parameters were varied within their statistical and systematic errors as given in Table 24 of the cited paper. It was investigated which parameters were the most important. It was found that the group of parameters describing the fragmentation process of light quarks (u,d,s) can be divided in two. The first group includes the parameters which are related to primary quark fragmentation, the second one includes parameters related to the fragmentation in general (perturbative and non-perturbative QCD processes). The most important parameters for the kaon production in the first group are the s-quark suppression (γ_s) and the probability that a strange meson will have spin 1 (V/(V+P+T)), in the second group the most important are $\Lambda_{\rm QCD}$, Q_0 (cut off of gluon/quark virtualities in the perturbative QCD process). The uncertainties on parameters of the last group give a negligible contribution to the systematic error because the extra kaons created due to changes in these parameters carry no information about charge of primary quark and this is the case for all flavours. This was checked on JETSET simulations varying $\Lambda_{\rm QCD}$ and Q_0: the corresponding changes in the s-asymmetry were less than 10^{-4}. The second parameter from the first group, the probability that strange meson will have spin 1, gives a shift in momentum spectrum of kaons which is approximately the same for all light quarks: softening or hardening the spectrum. The systematic error on the s-asymmetry is about 0.0002.

The systematic error on the s-asymmetry was expressed in terms of the s suppression factor giving $\Delta A^0_{s\bar{s}} = 0.17\ \Delta\gamma_s$ (see section 5.1). The DELPHI tuning paper [9] gives $\gamma_s = 0.307 \pm 0.007$ (stat) $^{+0.002}_{-0.017}$ (syst). Due to the presence of inconsistent kaon data the systematic error is asymmetric. Redoing the tuning of JETSET using more recent data [19] and replacing the inconsistent kaon data gives $\gamma_s = 0.285$, consistent with result obtained by the ALEPH collaboration [17]. The systematic error on γ_s is taken as the half value of the shift in γ_s from 0.307 to 0.285. Using the full ALEPH result for $\gamma_s = 0.285 \pm 0.004$ (stat) $\pm$ 0.014 (syst), gives the same total systematic error coming from γ_s. Also the varying of the parameters of the fragmentation leads to the change of $K^{\pm}/\pi^{\pm}$ ratio, which is related to the kaon purity. The variation of $K^{\pm}/\pi^{\pm}$ ratio was found to be at most 5%, which gives a systematic error on the s quark pole asymmetry of 0.0008. Thus the combined errors on the s quark pole asymmetry from light quark fragmentation are 0.0024.

(4) The light quark tag applied in the Barrel region yields uncertainties on $A^0_{s\bar{s}}$. First, the presence of secondary vertices (photon conversion and hyperon decay) which tends to bias P_E^+ towards low values. Following the same approach as that used in [20], the rate of photon conversion was varied by $\pm$30% and that of K^0_S and Λ decays by $\pm$10%. Futhermore, a possible source of errors is the gluon splitting mechanism which results in c and b quarks pairs in the fragmentation process. The $g \to c\bar{c}$ and $g \to b\bar{b}$ rates were

conservatively varied by $\pm 50\%$ in order to evaluate the effects on $A^0_{s\bar{s}}$. Then, the lifetimes of b hadrons and D mesons can change the fraction of rejected b and/or c events.

Finally, the impact parameter resolution affecting the light quark tag: a source of error is given by the quality of the simulation to describe the significance of the tracks; these are the residual discrepancies in the resolution of impact parameters for real and simulated tracks which are used to compute the probability P_E^+. An estimate of this error is obtained by comparing the probability computed using negative impact parameters P_E^- in the sample with the selection cut $P_E^+ > 0.15$, where the contribution of heavy flavours and secondary decay vertices to P_E^- is highly suppressed. The difference between the selection efficiencies computed using real and simulated distributions of P_E^- is used as an estimate on the uncertainty coming from the detector resolution on impact parameters.

Summing all contributions discussed above, the total systematic error on the s quark pole asymmetry, $A^0_{s\bar{s}}$, is 0.0034 for the barrel region and 0.0068 for the forward region. The systematic errors for the off peak points are the same.

5.3 Maximum likelihood method

The s quark asymmetry for data registered in 1994 and 1995 has also been measured with a maximum likelihood method which maximally exploits the information contained in the kaon momentum spectrum. The kaon selection and identification is identical to the one described in section 3.1. However, the light-quark tagging is not applied. In this analysis, each event is given probabilities to belong to six possible event classes, according to the kaon momentum. The classification is based on Monte Carlo results with full detector simulation, five of the classes being determined by the initial quark flavour (s,u,d,c or b) while class 6 contains events where the "kaon" is a misidentified particle. Figure 5 shows the fraction of events in each class, as expected from the full detector simulation, as a function of $\log p_K$ where p_K is the kaon momentum. For each year, probability tables were prepared on the basis of distributions like those in Figure 1. These tables were then used to determine the probabilities $\mathcal{P}_q(\log p_K)$ for a data event, characterised by the momentum p_K of the highest momentum charged kaon, to belong to the six different event classes.

The log-likelihood function $\mathcal{L}$ is defined as :

$$\mathcal{L} = -\sum_i \log\left[\sum_q \mathcal{P}_q(\log p_K)\frac{1}{2}\left(1 + \frac{8}{3} b_q A_{q\bar{q}} \frac{\cos\theta_q}{1+\cos^2\theta_q}\right)\right] \tag{22}$$

containing sums over all data events i and event classes q. θ_q is the polar angle of the primary quark, estimated from the direction of the thrust axis, oriented to point in the direction of the highest momentum charged kaon :

$$\cos\theta_q = -Q_K \cdot \cos\theta_{thrust} \quad . \tag{23}$$

$A_{q\bar{q}}$ is the asymmetry of class q and b_q are charge dilution factors related to the probability that the kaon by its charge and direction correctly distinguishes between the primary flavour and anti–flavour. The factor b_q is equal to $2c_q - 1$ in Eq.(5). The charge dilution factors for the five flavour classes are defined by :

$$b_q = \frac{N^-(\vec{p}_K\cdot\vec{p}_q > 0) + N^+(\vec{p}_K\cdot\vec{p}_q < 0) - N^-(\vec{p}_K\cdot\vec{p}_q < 0) - N^+(\vec{p}_K\cdot\vec{p}_q > 0)}{N^-(\vec{p}_K\cdot\vec{p}_q > 0) + N^+(\vec{p}_K\cdot\vec{p}_q < 0) + N^-(\vec{p}_K\cdot\vec{p}_q < 0) + N^+(\vec{p}_K\cdot\vec{p}_q > 0)} \tag{24}$$

and are parameterized as functions of $\log p_K$. The charge dilution of the "background class", class 6, is included in the background asymmetry (see below).

Systematic source	$\delta A_s^0\ (\times 10^{-4})$	
	Barrel	Forward
A_c^0 and A_b^0	16.5	26.7
Experimental asymmetry fit	11.9	25.8
$K^{\pm}$ momentum resolution	6.5	4.8
Total	21.4	37.4
$f(D^{\pm}) = 0.233 \pm 0.028$	0.2	0.4
$f(D^0) = 0.557 \pm 0.053$	7.3	15.2
$f(D_s) = 0.102 \pm 0.037$	5.6	12.0
$f(c_{bar}) = 0.065 \pm 0.029$	1.0	1.9
c hadrons decay multiplicity $= 2.35 \pm 0.06$	0.2	0.5
$< x_c >= 0.484 \pm 0.008$ (charm fragmentation)	1.2	2.3
$BR(D^0 \to K^- X) = 53 \pm 4\%$	2.5	5.0
$BR(D^0 \to K^+ X) = 3.4 + 0.6 - 0.4\%$	1.4	3.0
$BR(D^+ \to K^- X) = 24.2 \pm 2.8\%$	1.4	3.1
$BR(D^+ \to K^+ X) = 5.8 \pm 1.4\%$	2.2	4.7
$BR(D_s \to K^- X) = 13 + 14 - 12\%$	1.7	3.3
$BR(D_s \to K^+ X) = 20 + 18 - 14\%$	7.0	15.5
Total from c quark sector	12.4	26.5
b hadron decay multiplicity $= 5.73 \pm 0.35$	0.2	4.9
$< x_b >= 0.702 \pm 0.008$ (bottom fragmentation)	0.2	4.3
B_d mixing: $x_d = 0.70 \pm 0.04$	-	2.3
$BR(b \to K^{\pm} X) = 88 + 12 - 19\%$	1.4	34.6
$f(B^{\pm}) = 37.8 \pm 2.2\%$	0.2	4.7
$f(B^0) = 37.8 \pm 2.2\%$	0.1	1.2
$f(B_s) = 11.2 \pm 1.9\%$	0.2	3.5
$f(b_{bar}) = 13.2 \pm 4.1\%$	0.1	2.0
$BR(B^0 \to K^- X) = 0.13 \pm 0.04$	0.9	17.9
$BR(B^0 \to K^+ X) = 0.73 \pm 0.08$	0.2	6.2
$BR(B^+ \to K^- X) = 0.13 \pm 0.05$	0.5	11.7
$BR(B^+ \to K^+ X) = 0.58 \pm 0.08$	0.3	8.5
$BR(D_s \to K^- X)$ from b quark	0.3	7.9
$BR(D_s \to K^+ X)$ from b quark	0.1	1.6
Total from b quark sector	1.9	43.8
Impact parameters resolution	0.3	-
photon conversion $\pm 30\%$	1.2	-
$K_S^0(u, d, s) \pm 10\%$	0.3	-
$\Lambda(u, d, s) \pm 10\%$	0.3	-
$g \to c\bar{c} \pm 50\%$	0.5	-
$g \to b\bar{b} \pm 50\%$	0.1	-
b hadrons lifetimes	0.1	-
D mesons lifetimes	0.1	-
Total uncertainties from light quark tag	1.4	-
Statistical error on γ_s	11.9	11.9
Shift in γ_s	18.7	18.7
Variation of the K/π ratio	7.8	7.8
light quark fragmentation	23.5	23.5
Total systematic error	34.2	67.6

Table 10: Summary of the systematic errors on s quark pole asymmetry using the Standard Model values for the up and down quark pole asymmetry.

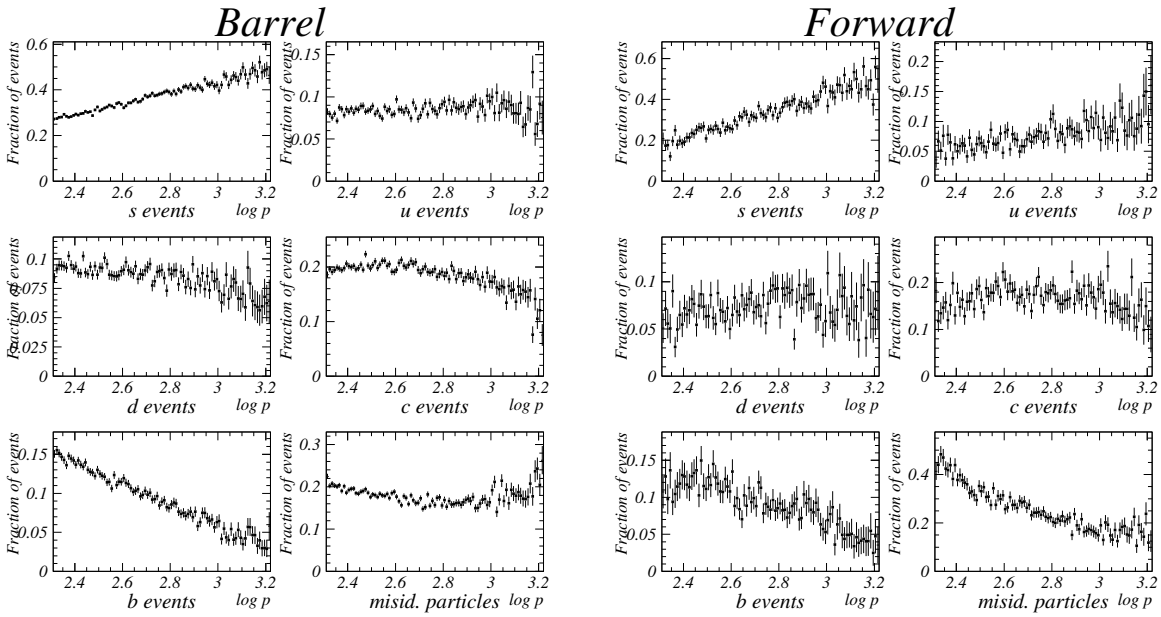

Figure 5: The sample fraction as a function of the kaon momentum for the six event classes, given by the full detector simulation for events with kaons identified by the Barrel (left) and Forward (right) RICH. (1994 DELSIM Monte Carlo.)

For the five flavour classes, the peak asymmetries $A_{q\bar{q}}$ in Eq. (22) are obtained from the pole asymmetries taking into account the radiative corrections. The analysis uses the measured pole and off-peak asymmetries for b and c quarks [1] and the assumptions $A_{FB}^{u\bar{u}} = A_{FB}^{c\bar{c}}$ and $A_{FB}^{d\bar{d}} = A_{FB}^{b\bar{b}}$. To investigate the influence of these constraints, the input value of $A_{d\bar{d}}^0$ is varied in the interval $A_{b\bar{b}}^0 \pm 10\sigma$, where σ is the uncertainty in the measurement of $A_{b\bar{b}}^0$, keeping $A_{u\bar{u}}^0$ fixed. In a similar way the value of $A_{u\bar{u}}^0$ is varied within $A_{c\bar{c}}^0 \pm 10\sigma$, where σ is the uncertainty in the measurement of $A_{c\bar{c}}^0$, with $A_{d\bar{d}}^0$ fixed.

The asymmetry of class 6, A^{bckg}, is estimated from the full detector simulation. With a total number of events n_{bckg} in the class out of which n_{bckg}^q originate from quark flavour q, the asymmetry was calculated as

$$A_{\mathrm{FB}}^{bckg} = \sum_q \frac{n_{bckg}^q}{n_{bckg}} b_q A_{q\bar{q}} \quad . \tag{25}$$

The sum is over all the quark flavours. b_q are charge dilution factors, calculated using equation (24) for the sample of misidentified particles. The resulting background asymmetries are negligible in all cases.

The performance of the maximum likelihood algorithm depends on how well the kaon identification for real data is represented by the Monte Carlo. Studies to determine how often a pion is misidentified as a kaon were therefore performed, using pions from reconstructed K_S^0 decays and high purity muons identified by the muon chambers and the ionization energy loss measured in the TPC. The misidentification probability for high momentum muons in the RICH is expected to be the same as for isolated pions. The observed discrepancies in kaon misidentification between data and simulation were then corrected applying weights to simulated events where the high momentum kaon actually was a misidentified pion. The effect of the uncertainties in the applied weights due to

Systematic source	δA_s^0 ($\times 10^{-4}$)	
	Barrel	Forward
kaon purity	14.8	16.7
background asymmetry	4.6	10.1
Kaon identification uncertainties, total	15.5	19.5
thrust axis reconstruction	0.9	0.2
limited Monte Carlo statistics	5.9	60.1
$A_{FB}^{b,\bar{b}}$ and $A_{FB}^{c,\bar{c}}$	19.1	13.7
Fit method, total	20.0	61.6
D hadron production	4.1	5.8
D hadron decays	7.0	11.1
B hadron production	2.9	2.8
B hadron decays	30.0	23.9
fragmentation description	14.0	14.0
shift in γ_s	18.7	18.7
Theoretical uncertainties, total	39.0	35.8
Total systematic uncertainty	46.5	73.9

Table 11: Contributions from various sources to the systematic uncertainty in the measured forward-backward asymmetry.

the limited statistics of the K_S^0 and the muon samples is included in the total systematic uncertainty.

Also, the influence of the difference in nuclear cross-section of K^+ and K^- on the measured asymmetry was investigated. An additional term, $A^{mat}(\theta)$, was introduced in equation (22), however the effect on the measured forward-backward asymmetries was negligible ($< 10^{-4}$). The possible effects of the momentum dependence of the K^+ and the K^- cross-sections were estimated to be negligible over the momentum range considered and therefore not taken into account in the analysis.

The systematic uncertainties are summarised in Table 11 which comprises uncertainties related to kaon identification, detector effects, the fit method and theoretical uncertainties including those due to the hadronisation model. The uncertainties due to the fragmentation process were evaluated using the method described in [9]. In some cases the contributions to the systematic uncertainties for the barrel and forward analyses are correlated. The correlation was found to be 62.0%.

Finally

$$A_{s\bar{s}}^0 = 0.103 \pm 0.012(\text{stat.}) \pm 0.005(\text{syst.}) \quad , \tag{26}$$

where the central value corresponds to $\gamma_s = 0.285$ and the systematic error allows for the shift in γ_s discussed in Section 5.1. This result has been corrected for the effects of the variation of the kaon misidentification probability with polar angle (a correction by less than 0.001).

The variation of $A_{s\bar{s}}^0$ with $A_{d\bar{d}}^0$ and $A_{u\bar{u}}^0$ can be included by adding to the above result two linear terms :

$$\mathcal{F}_d = 0.0103 \frac{A_{d\bar{d}}^0 - 0.0990}{0.0990} \tag{27}$$

$$\mathcal{F}_u = 0.0116 \frac{A_{u\bar{u}}^0 - 0.0709}{0.0709} \quad . \tag{28}$$

$\sqrt{s}$ (GeV)	89.5	91.2	93.0
$A_{FB}^{s\bar{s}}$	0.060 ± 0.047	0.098 ± 0.012	0.090 ± 0.039

Table 12: Summary of the determination of $A_{FB}^{s\bar{s}}$ for the 1992-1995 data. The errors correspond to the statistical and systematical errors combined.

For 1995, the data allow the determination of off-peak asymmetries. Applying the same shift in γ_s and in $A^0_{s\bar{s}}$ as above, the result is

$$A_{FB}^{s\bar{s}}(89.5 \text{ GeV}) = 0.062 \pm 0.048(\text{stat.}) \pm 0.020(\text{syst.}) \quad (29)$$
$$A_{FB}^{s\bar{s}}(93.0 \text{ GeV}) = 0.102 \pm 0.040(\text{stat.}) \pm 0.018(\text{syst.}) \quad . \quad (30)$$

The contributions to the systematic uncertainties for the off-peak results come from the same main sources as for the peak measurements.

6 Combined results and discussion

A measurement of the s quark forward-backward $A_{FB}^{s\bar{s}}$ and pole asymmetry $A^0_{s\bar{s}}$ has been performed using 3.2 M hadronic Z events. Charged kaons identified in the Barrel and Forward RICH are used to determine the kaon asymmetry. From the kaon asymmetry, fixing asymmetries and production fractions for the up, down, charm and bottom quarks to the Standard Model values, the s quark forward-backward asymmetries combining the barrel and forward results for different centre-of-mass energies are evaluated and shown in Table 12 and in Figure 6 together with the Standard Model prediction. For the modelling of the fragmentation of quarks the JETSET 7.3 model was used, tuned to LEP data. The systematic errors have been estimated including errors coming from the uncertainties on the tuned JETSET parameters. Correlations between the errors in the barrel and forward regions have been taken into account.

The $s\bar{s}$ asymmetry at a centre-of-mass energy of 91.2 GeV as a function of the polar angle is shown in Figure 7.

Fixing $A^0_{d\bar{d}}, A^0_{u\bar{u}}$ to the Standard Model values of 0.1031 and 0.0736 respectively and $A^0_{b\bar{b}}$ and $A^0_{c\bar{c}}$ to the measured values, gives for the s quark pole asymmetry: $A^0_{s\bar{s}} = 0.1008 \pm 0.0113\,(\text{stat.}) \pm 0.0040\,(\text{syst.})$. The s quark pole asymmetry as a function of the up and down quark asymmetries can be written as

$$A^0_{s\bar{s}} = 0.1008 \pm 0.0113\,(\text{stat.}) \pm 0.0040\,(\text{syst.}) \quad (31)$$
$$+0.0121\frac{A^0_{d\bar{d}} - 0.1031}{0.1031} + 0.0115\frac{A^0_{u\bar{u}} - 0.0736}{0.0736}$$

For the data collected in 1994 and 1995, the pole asymmetry and the off-peak asymmetries have also been measured using a maximum likelihood method. The results obtained are consistent. The predicted pole asymmetry for up, down and strange quarks was calculated from the effective electroweak mixing angle using Eqs.(5) and (6) using as a constraint the experimental result given in Eq.(31). The effective electroweak mixing angle corresponds to :

$$\sin^2\theta^{lept}_{eff} = 0.2321 \pm 0.0029 \quad (32)$$

Assuming the values for the up and down quark asymmetries from the Standard Model and using for A_e the measured value of 0.1479 ± 0.0051 [1], the parity violating coupling of the s quark to the Z is determined from Eq.(5) to be:

$$A_s = 0.909 \pm 0.102\,(\text{stat.}) \pm 0.036(\text{syst.}). \tag{33}$$

The experimental result on the s quark asymmetry is compatible with our previous result [3] and with the s quark forward-backward asymmetry measured by OPAL collaboration. Both the statistical and systematic errors are smaller than those of the model independent analysis from OPAL [4].

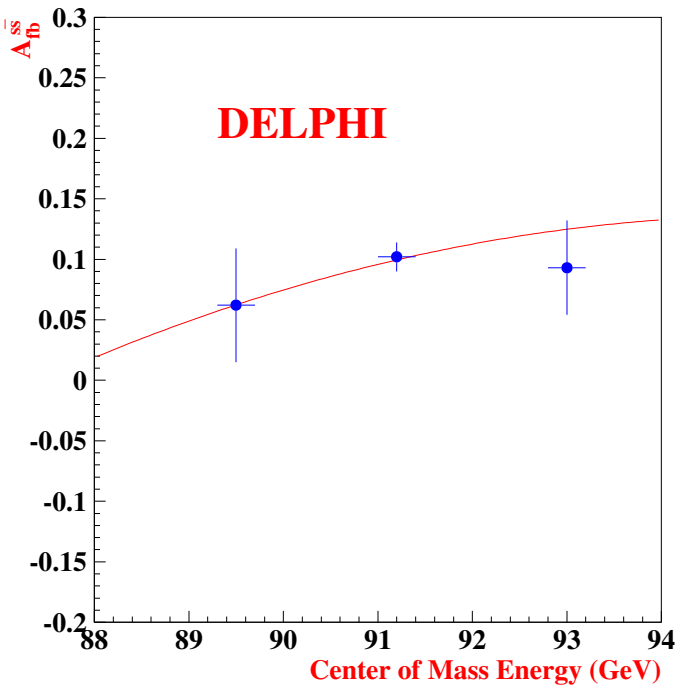

Figure 6: The measured s quark forward-backward asymmetry as a function of the centre-of-mass energy. The points correspond to the data, the curve to the Standard Model expectation (ZFITTER: $M_{\mathrm{Z}} = 91.1866$ GeV/c^2, $m_t = 173$ GeV/c^2, $m_H = 115$ GeV/c^2)

The s quark pole asymmetry can be compared to the measured pole asymmetry for b quarks at LEP of 0.0990 ± 0.0021 (Eq.(7)). The Standard Model predicts the same asymmetries (see introduction) for strange and bottom quarks. This measurement is compatible with the hypothesis of the flavour independence of the asymmetry for bottom and strange quarks. The measured s quark asymmetries and the parity violating coupling of the s quark to the Z agree with the Standard Model expectations.

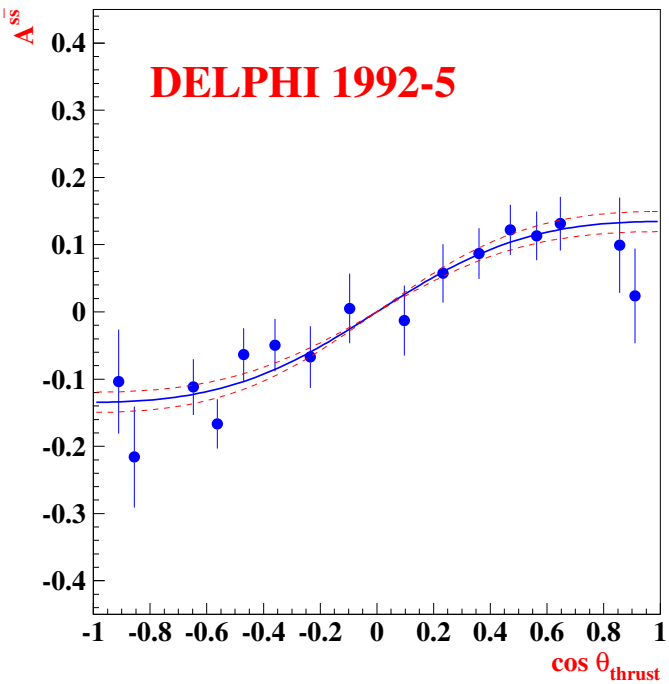

Figure 7: The s quark asymmetry as a function of $\cos\theta_{thrust}$. The data points are the values computed from the measured kaon asymmetry, the errors are statistical only. The superimposed curve represents the result of the measurement $A_{FB}^{s\bar{s}}$ at 91.2 GeV (see Table 12), the dashed curves correspond to one standard deviation.

Acknowledgements

We are greatly indebted to our technical collaborators, to the members of the CERN-SL Division for the excellent performance of the LEP collider, and to the funding agencies for their support in building and operating the DELPHI detector.
We acknowledge in particular the support of
Austrian Federal Ministry of Science and Traffics, GZ 616.364/2-III/2a/98,
FNRS–FWO, Belgium,
FINEP, CNPq, CAPES, FUJB and FAPERJ, Brazil,
Czech Ministry of Industry and Trade, GA CR 202/96/0450 and GA AVCR A1010521,
Danish Natural Research Council,
Commission of the European Communities (DG XII),
Direction des Sciences de la Matière, CEA, France,
Bundesministerium für Bildung, Wissenschaft, Forschung und Technologie, Germany,
General Secretariat for Research and Technology, Greece,
National Science Foundation (NWO) and Foundation for Research on Matter (FOM), The Netherlands,
Norwegian Research Council,
State Committee for Scientific Research, Poland, 2P03B06015, 2P03B1116 and SPUB/P03/178/98,
JNICT–Junta Nacional de Investigação Científica e Tecnológica, Portugal,
Vedecka grantova agentura MS SR, Slovakia, Nr. 95/5195/134,
Ministry of Science and Technology of the Republic of Slovenia,
CICYT, Spain, AEN96–1661 and AEN96-1681,
The Swedish Natural Science Research Council,
Particle Physics and Astronomy Research Council, UK,
Department of Energy, USA, DE–FG02–94ER40817.

References

[1] The LEP Collaborations, the LEP Electroweak Working Group and the SLD Heavy Flavour Group, "*A Combination of Preliminary Electroweak Measurements and Constraints on the Standard Model*", CERN-PPE/99-15 (1999).

[2] G. Altarelli, R. Kleiss and C. Verzegnassi (eds.), " Z Physics at LEP 1 ", CERN 89-08 vol 1, p 203.

[3] P. Abreu et al., DELPHI Coll., Z. Phys. **C67** (1995) 1.

[4] K. Ackerstaff et al., OPAL Coll., Z. Phys. **C76** (1997) 387.

[5] P. Aarnio et al (DELPHI Coll.), Nucl. Instr. and Meth. **A303** (1991) 233.

[6] E.G. Anassontzis et al., Nucl. Instr. and Meth. **A323** (1992) 351.

[7] W. Adam et al., Nucl. Instr. and Meth. **A338** (1994) 284.

[8] T. Sjöstrand, Comp. Phys. Comm. **82** (1994) 74.

[9] P. Abreu et al., DELPHI Coll., Z. Phys. **C73** (1996) 11.

[10] "*DELSIM User Manual*", DELPHI 87-96/PROG 99 (1989);
"*DELSIM Reference Manual*", DELPHI 87-98/PROG 100 (1989).

[11] M.Battaglia and P.M.Kluit, Nucl. Instr. and Meth. **A433** (1999) 47.

[12] D. Bloch, M. Dracos, S. Tzamarias, Nucl. Instr. and Meth. **A371** (1995) 236.

[13] G. Borisov and C. Mariotti, Nucl. Instr. and Meth. **A372** (1996) 181.

[14] D. Bardin et al., Z. Phys. **C44** (1989) 493; D. Bardin et al., Comp. Phys. Comm. **59** (1990) 303; D. Bardin et al., Nucl. Phys. **B351** (1991) 1; D. Bardin et al., Phys. Lett. **B255** (1991) 290; D. Bardin et al., CERN-TH 6443/92 (1992).

[15] Particle Data Group, The European Physical Journal **C3** (1998) 1.

[16] The LEP/SLD Heavy Flavour Working Group, *Electroweak Heavy Flavour Results presented at the 1999 Winter Conferences*", LEPHF/99-01.
The LEP/SLD Heavy Flavour Working Group, *Input parameters for the LEP/SLD Electroweak Heavy Flavour Results for Summer 1998 Conferences*", LEPHF/98-01.
D. Abbaneo et al, Eur. Phys. J. C4 (1998) 2, 185.

[17] R. Barate et al., ALEPH Coll., Phys. Rep. 294 (1998) 1.

[18] H. Albrecht et al., ARGUS Coll., Z. Phys. **C62** (1994) 371.

[19] P. Abreu et al., DELPHI Coll., E. Phys. J. **C5** (1998) 585.

[20] P. Abreu et al., DELPHI Coll., Z. Phys. **C66** (1995) 323.